Journal of Applied Physics

RESEARCH ARTICLE | JUNE 03 2024

The effects of high-pressure annealing on magnetostructural transitions and magnetoresponsive properties in stoichiometric MnCoGe

Tej Poudel Chhetri ; Jing-Han Chen ; David P. Young ; Igor Dubenko ; Saikat Talapatra ; Naushad Ali ; Shane Stadler

Check for updates

J. Appl. Phys. 135, 215101 (2024)
https://doi.org/10.1063/5.0204371

View Online
Export Citation

Articles You May Be Interested In

The influence of hydrostatic pressure and annealing conditions on the magnetostructural transitions in MnCoGe

J. Appl. Phys. (June 2021)

Giant magnetocaloric effects by tailoring the phase transitions

Appl. Phys. Lett. (April 2010)

Negative thermal expansion and magnetocaloric effect in Mn-Co-Ge-In thin films

Appl. Phys. Lett. (January 2018)

26 December 2024 02:38:23

AIP Publishing

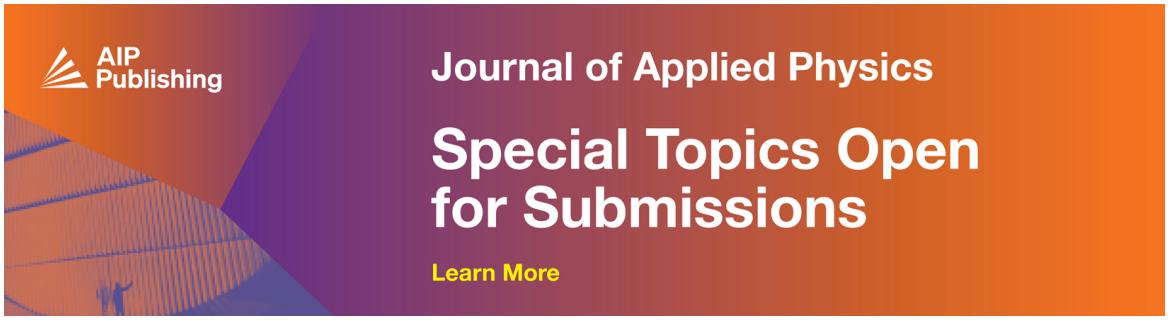

AIP Publishing

Journal of Applied Physics ARTICLE pubs.aip.org/aip/jap

The effects of high-pressure annealing on magnetostructural transitions and magnetoresponsive properties in stoichiometric MnCoGe

Cite as: J. Appl. Phys. **135**, 215101 (2024); doi: 10.1063/5.0204371
Submitted: 21 February 2024 · Accepted: 21 May 2024 ·
Published Online: 3 June 2024

View Online Export Citation CrossMark

Tej Poudel Chhetri,[1,a)] Jing-Han Chen,[1] David P. Young,[1] Igor Dubenko,[2] Saikat Talapatra,[2] Naushad Ali,[2] and Shane Stadler[1]

AFFILIATIONS

[1]Department of Physics and Astronomy, Louisiana State University, Baton Rouge, Louisiana 70803, USA
[2]School of Physics and Applied Physics, Southern Illinois University, Carbondale, Illinois 62901, USA

[a)]**Author to whom correspondence should be addressed:** tpoude1@lsu.edu

ABSTRACT

In this study, phase transitions (structural and magnetic) and associated magnetocaloric properties of stoichiometric MnCoGe have been investigated as a function of annealing pressure. Metastable phases were generated by annealing at 800 °C followed by rapid cooling under pressures up to 6.0 GPa. The x-ray diffraction results reveal that the crystal cell volume of the metastable phases continuously decreases with increasing thermal processing pressure, leading to a decrease in the structural transition temperature. The magnetic and structural transitions merge and form a first-order magnetostructural transition between the ferromagnetic orthorhombic and paramagnetic hexagonal phases over a broad temperature range (>80 K) spanning room temperature, yielding considerable magnetic entropy changes. These findings demonstrate the utility of thermal processing under high pressure, i.e., high-pressure annealing, to control the magnetostructural transitions and associated magnetocaloric properties of MnCoGe without altering its chemical composition.

© 2024 Author(s). All article content, except where otherwise noted, is licensed under a Creative Commons Attribution (CC BY) license (https://creativecommons.org/licenses/by/4.0/). https://doi.org/10.1063/5.0204371

26 December 2024 02:38:23

I. INTRODUCTION

Ternary intermetallic compounds of the general formula Mn*TX* (*T* = Ni, Co and *X* = Si, Ge) are versatile materials that possess multifunctional magnetoresponsive properties, including magnetocaloric effects (MCEs),[1–5] magnetic shape memory effects,[6] colossal magnetoresistance,[7] and negative thermal expansion,[8–10] all of which have fundamental and practical significance. Among these effects, the MCE is a particularly attractive functional property because it is the basis of energy-efficient magnetic cooling systems, which may be the future replacement of conventional vapor-compression cooling technology. The functional properties of Mn*TX* compounds often originate from the strong interplay between the lattice and spin degrees of freedom, i.e., a coupling of the magnetic and structural transitions.[11] A challenge, however, is that these compounds undergo magnetic and structural transitions at different temperatures in their stoichiometric forms (i.e., the magnetic and structural properties are initially uncoupled), with the structural transitions occurring at significantly higher temperatures.[12–14] Therefore, substantial efforts have been made to tune the phase transitions in these materials to create a magnetostructural transition (MST) and understand its physical mechanisms, as a proper understanding of the MST process will aid in tailoring their functional properties and may reveal novel physical behaviors.

The magnetic and crystallographic stabilities of Mn*TX* compounds are sensitive to the covalent bonding between the *T* and *X* atoms and the interatomic distance between neighboring Mn atoms.[15,16] Hence, their phase transitions (magnetic and structural) can be tuned by manipulating the interatomic spacing and bonding, which has been done extensively via elemental

© Author(s) 2024

substitution,[17–28] isostructural alloying,[29–32] and stoichiometric variations.[33–36] These tuning strategies have resulted in coupled magnetostructural transitions near room temperature, along with large magnetoresponsive effects, in many of these materials. However, in some cases, excessive levels of doping or alloying of the parent compound are required,[37,38] which may generate undesired effects, such as reducing the magnetic moment, which can diminish the magnetocaloric effects.

The composition-variation technique is not the sole route for tuning the phase transitions. The application of external hydrostatic pressure, i.e., physical pressure, during measurement can also drive the structural transition to lower temperatures, resulting in coupled magnetostructural transitions in materials without changing their compositions.[39–41] However, the shifts in transitions due to the physical pressure are temporary, i.e., the transitions return to their original temperatures after the removal of the applied hydrostatic pressure, in contrast to chemical pressure (doping, substitutions, and interstitial elements), which permanently shifts the transitions.[42,43] In some cases, couplings between the magnetic and structural transitions have been realized through post-synthesis processing such as thermal annealing or quenching.[44–49] A strategy of size reduction, i.e., the synthesis of micro- and nanomaterials,[50] or the growth of thin films or ribbons[51–53] has also been employed to manipulate the phase transitions and associated magnetocaloric properties. Despite these various tuning strategies, the exploration of novel and effective approaches for coupling the magnetic and structural transitions in potential magnetocaloric materials is actively ongoing for the optimization of their magnetoresponsive properties.

High-pressure techniques may serve as effective methods for manipulating the structure and properties of materials. High pressure can modify the micro- and macrostructures of a material by inducing atomic rearrangement, which is reflected in changes in physical properties.[54] Therefore, many solids form new phases under high pressure/temperature that are not obtained at ambient conditions, which may be preserved as "metastable phases" upon cooling and decompression. These new phases often possess useful and different properties than their original stable phases, which may enhance properties, or reveal new phenomena. Although high-pressure techniques are capable of tuning the properties of materials, their use in producing magnetocaloric materials has not been fully explored.[55–59] Hence, we investigated the effects of high-pressure annealing on the phase transitions and associated magnetoresponsive properties of a specific member of the Mn*TX* family.

The material of interest in the present study is stoichiometric MnCoGe, which undergoes a structural phase transition from a high-temperature Ni_2In-type hexagonal structure (space group:$P6_3/mmc$) to a low-temperature TiNiSi-type orthorhombic structure (space group: *Pnma*) around $T_M \sim 420$ K, as shown in Fig. 1.[23] It further exhibits a magnetic phase transition between the ferromagnetic (FM) and paramagnetic (PM) states at $T_C \sim 345$ K.[60] A promising feature of this material is that its structural transition is sensitive to both physical and chemical pressures, enabling the modification of its properties utilizing these stimuli.[42] Here, we generated a series of metastable phases of MnCoGe by annealing at 800 °C followed by rapid cooling under different pressures up to 6 GPa and investigated their phase transitions (magnetic and structural) and associated magnetocaloric properties. When thermal processing occurred under high pressure, the structural transition shifted markedly toward lower temperature, leading to a coupling of the magnetic and structural transitions near room temperature, which resulted in considerable magnetocaloric effects. It was found that this first-order MST could be tuned over a wide range of temperatures by varying the thermal processing pressure. These results illustrate that stoichiometric MnCoGe with negligible MCE at room temperature (when synthesized using conventional techniques at ambient pressure) can be transformed into an effective room-temperature magnetocaloric material by forming metastable phases through high-pressure annealing without changing its chemical composition.

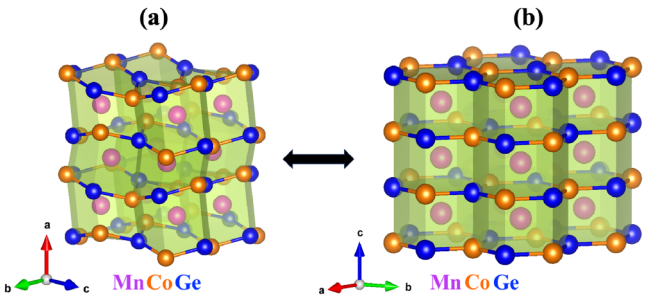

FIG. 1. (a) Orthorhombic and (b) hexagonal phases of stoichiometric MnCoGe drawn in a polyhedral view using VESTA software.[61] The structural phase transition in MnCoGe occurs between these low-temperature orthorhombic and high-temperature hexagonal phases.

II. EXPERIMENTAL DETAILS

To fabricate a polycrystalline sample with a nominal composition of MnCoGe, an appropriate amount of the constituent elements with purities better than 99.9% were first placed in an Al_2O_3 crucible and sealed in a quartz tube under vacuum. The quartz tube sample assembly was then heated to 1100 °C for 12 h in a tube furnace to form MnCoGe, as the complete liquefaction of components of MnCoGe occurs at this temperature.[48] The so-formed ingot was re-melted at 1100 °C for another 12 h to ensure homogeneity and slowly cooled to room temperature in 24 h. The ingot was then ground into powder, which was used as the source material for samples subjected to subsequent heat and pressure treatments.

Two-gram samples of the source material were sealed in two evacuated quartz tubes and annealed at 800 °C for 36 h at atmospheric pressure. The sample labeled SC_0 was then slowly cooled to room temperature at a rate of 0.5 °C/min, while the sample labeled RC_0 was rapidly cooled (i.e., quenched) by immersing it in liquid nitrogen.

Thermal processing under high pressure was carried out using a cubic multi-anvil apparatus manufactured by Rockland Research Corporation. Initially, about 0.5 g of the source powder material was pressed into a pellet of 6 mm diameter and put in a boron nitride (BN) crucible, which was then placed in a graphite tube

26 December 2024 02:38:23

© Author(s) 2024

TABLE I. Thermal processing parameters of all samples. The thermomagnetic properties for a field change of 7 T are shown for two samples.

Composition	Labels	Annealing temperature (°C)	Pressure (GPa)	Cooling process	T_M (K)	$-\Delta S_M$ (J kg^{-1} K^{-1})	δ_{FWHM} (K)	*RCP* (J/kg)
	SC_0	800	Ambient	Slowly cooled	429	…	…	…
	RC_0	800	Ambient	Rapidly cooled	334	…	…	…
MnCoGe	RC_1.2	800	1.2	Rapidly cooled	271	11.4	30	342
	RC_2.2	800	2.2	Rapidly cooled	267	10	42	420
	RC_3.5	800	3.5	Rapidly cooled	263	…	…	…
	RC_6.0	800	6.0	Rapidly cooled	254	…	…	…

sealed with pyrophyllite lids at both ends. The graphite tube was subsequently positioned inside a pyrophyllite cube, serving as the medium for transmitting pressure. The temperature was monitored using a thermocouple fitted within the pyrophyllite cube. The entire sample assembly was compressed to the desired pressure and then heated to 800 °C for 1 h at that pressure. Subsequently, the sample was rapidly cooled to ambient temperature by powering off the heat source, and decompression occurred after a 3 h wait time. Employing this process, the samples labeled RC_1.2, RC_2.2, RC_3.5, and RC_6.0 were prepared under pressures of 1.2, 2.2, 3.5, and 6.0 GPa, respectively. Note that "SC" and "RC" in the sample labels stand for "slowly cooled" and "rapidly cooled," respectively, and the numbers (0, 1.2, 2.2, 3.5, and 6.0) indicate the magnitude of pressure (in GPa) under which the thermal-pressure processing occurred. The details of the processing conditions of all samples are summarized in Table I.

The crystal structures and phase compositions of all samples at room temperature were identified through powder x-ray diffraction (XRD) using a Scintag XDS2000 powder diffractometer (Cu Kα radiation). Rietveld refinements of the XRD patterns were carried out using General Structure Analysis System (GSAS) software[62,63] to extract crystallographic parameters, including lattice constants and unit cell volumes. Heat flow measurements were conducted using a differential scanning calorimeter (SDT Q600 model from TA Instruments, Inc.) to determine the structural transition characteristic temperatures above 400 K. The magnetization measurements were performed using a Magnetic Property Measurement System (MPMS) manufactured by Quantum Design at temperatures ranging from 100 to 400 K and applied magnetic fields up to 7 T.

III. RESULTS AND DISCUSSION

The room-temperature XRD patterns of MnCoGe annealed at 800 °C followed by either slow or rapid cooling under various pressures are shown in Fig. 2. According to these results, MnCoGe, when slowly cooled at atmospheric pressure, i.e., sample SC_0, displayed a TiNiSi-type orthorhombic structure, which is consistent with the previous report.[12] Furthermore, the XRD patterns of MnCoGe when rapidly cooled at ambient pressure, i.e., sample RC_0, could also be indexed in the orthorhombic structure. However, a combination of the TiNiSi-type orthorhombic and Ni_2In-type hexagonal structures was observed when the rapid cooling occurred under 1.2 GPa pressure (RC_1.2), where the dominant phase is the hexagonal phase (weight fraction = 0.874). This coexistence of both high- and low-temperature phases suggests that the structural transition temperature is close to room temperature (i.e., since the XRD data were collected at room temperature). Moreover, when rapidly cooled from 800 °C under pressures of

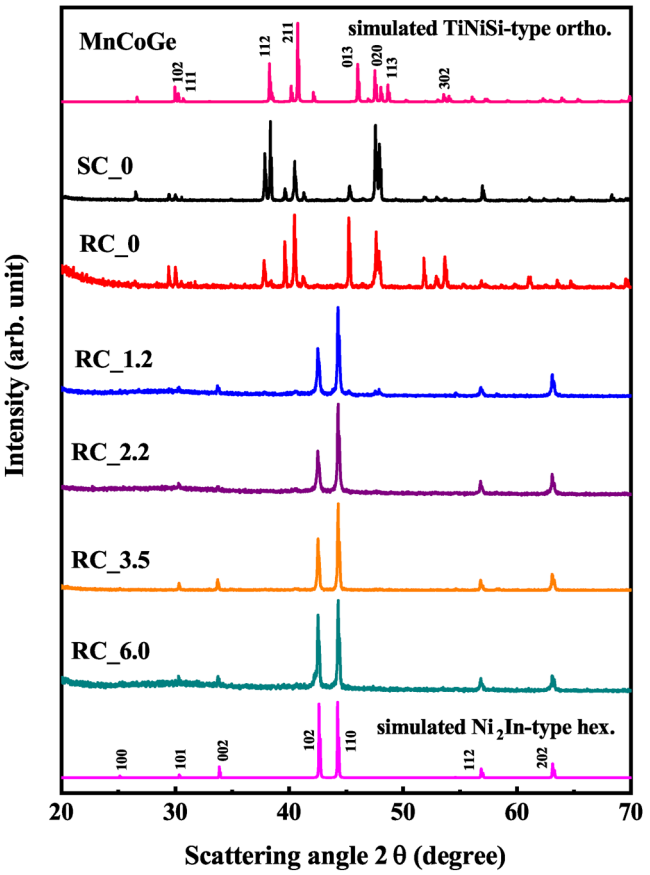

FIG. 2. Room-temperature XRD patterns for MnCoGe thermally processed under different pressures. The top and bottom patterns depict the ideal (calculated) XRD patterns for TiNiSi-type orthorhombic and Ni_2In-type hexagonal structures for comparison with experimental results.

26 December 2024 02:38:23

© Author(s) 2024

2.2 GPa or above (RC_2.2, RC_3.5, and RC_6.0), MnCoGe crystallized in the Ni_2In-type hexagonal structure. These results demonstrate that an increase in thermal processing pressure continuously shifts the structural transition to lower temperature, eventually stabilizing the high-temperature hexagonal phase near room temperature. A similar result of hexagonal-phase stabilization at room temperature in MnCoGe has been observed for higher thermal processing temperatures at ambient pressure.[44,47,48]

The XRD data were further analyzed through Rietveld refinements to determine the lattice parameters and cell volumes per formula unit for each sample, as presented in Table II. Figure 3 shows the variation of refined lattice parameters of the orthorhombic and hexagonal structures as a function of annealing pressure. Note that the TiNiSi-type orthorhombic structure is regarded as a distortion of the Ni_2In-type hexagonal structure, where their axes are related by $a_{ortho} \approx c_{hex}$, $b_{ortho} \approx a_{hex}$, and $c_{ortho} \approx \sqrt{3}\, a_{hex}$.[64–66] As the thermal processing pressure increased from 0 to 1.2 GPa, a_{ortho} decreased by ~10.6%, while b_{ortho} increased by ~6.8%. However, c_{ortho} changed minimally (~0.4%) relative to that of a_{ortho} and b_{ortho}. These deformations of the lattice parameters suggest that a significant reconstruction of the crystal structure occurs during the structural transition. As a consequence, a large change in unit cell volume (~4.2%), as shown in Fig. 4, was observed when MnCoGe changed its crystallographic configuration from the orthorhombic to the hexagonal structure. Such a significant change in crystal volume suggests that the transition may be easily influenced by hydrostatic pressure, and the material is likely to exhibit a giant barocaloric effect.[65] Furthermore, the unit cell volume in the hexagonal phase continuously decreased with increasing annealing pressure (see Fig. 4). This crystal volume reduction may change the interlayer distance and covalent bond between the Mn–Mn atoms, which are largely responsible for shifting the structural transition to a lower temperature.[15]

Figure 5 displays the magnetization measurements as a function of temperature for all samples carried out with field-cooled cooling (FCC) and field-cooled warming (FCW) protocols in an applied magnetic field of $\mu_0 H = 0.1$ T. For MnCoGe slowly cooled at atmospheric pressure, i.e., sample SC_0, a thermally reversible magnetic transition from a high-temperature PM to a low-temperature FM state was observed at T = 350 K. Its structural transition was investigated using DSC measurements, as shown in the upper right curves in Fig. 5 because it occurs at a temperature significantly higher than room temperature and in the

TABLE II. The structural parameters of all MnCoGe samples, including their primary crystal structures, lattice constants, and cell volumes per formula unit, determined through Rietveld refinements of the XRD data collected at room temperature.

Labels	Phase	a (Å)	b (Å)	c (Å)	Vol./f.u. (Å^3)
SC_0	Ortho.	5.9535	3.8216	7.0528	40.117
RC_0	Ortho.	5.9472	3.8248	7.0528	40.108
RC_1.2	Hex.	4.0871	4.0871	5.3128	38.428
RC_2.2	Hex.	4.0869	4.0869	5.3125	38.424
RC_3.5	Hex.	4.0854	4.0854	5.3109	38.383
RC_6.0	Hex.	4.0848	4.0848	5.3086	38.355

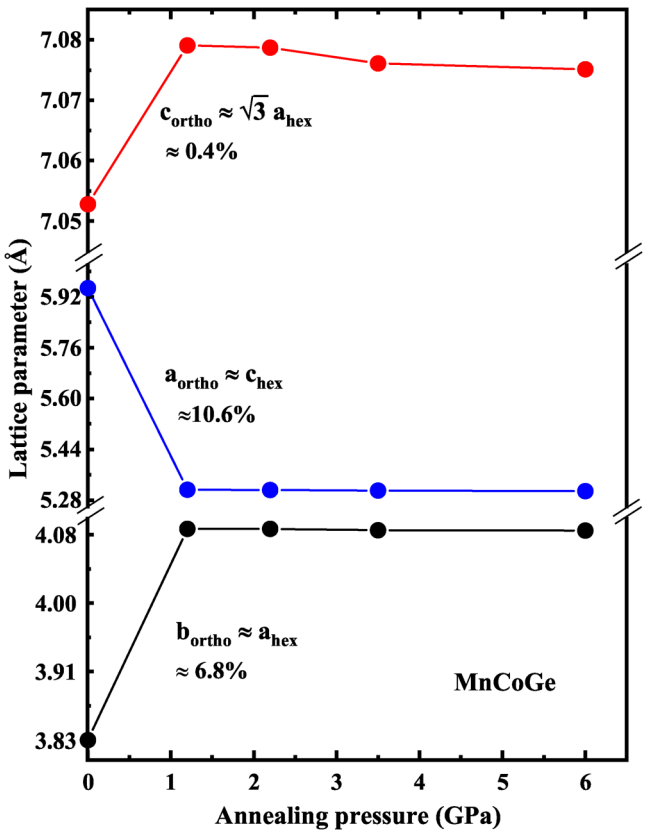

FIG. 3. Lattice parameters at room temperature as a function of annealing pressure for MnCoGe annealed at 800 °C followed by rapid cooling under various pressures.

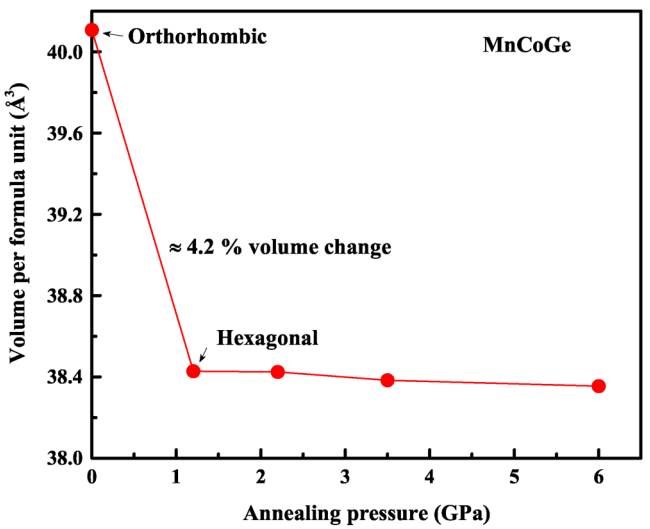

FIG. 4. Pressure-dependent cell volume per formula unit for MnCoGe. The cell volumes decrease as the annealing pressure increases.

26 December 2024 02:38:23

© Author(s) 2024

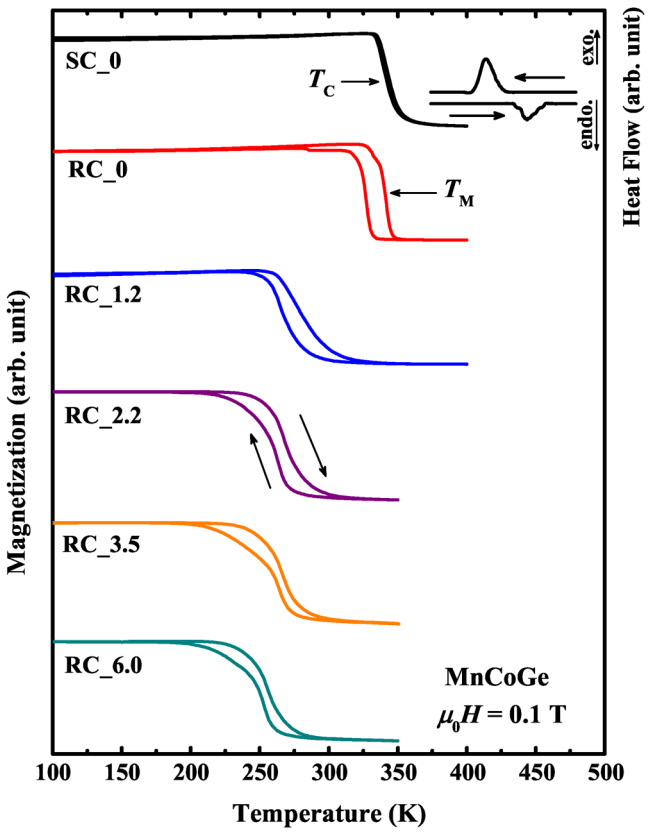

FIG. 5. Magnetization as a function of temperature for all samples measured in an applied field of $\mu_0 H = 0.1$ T using FCC and FCW protocols. The arrows in the graph indicate the directions of the heating and cooling paths. The baseline-corrected DSC measurements, as shown in upper right curves, were performed to detect the structural transition in the sample SC_0, as it occurs at a temperature significantly higher than room temperature, and is not detectable in the magnetization measurement. An increase in annealing pressure continuously shifted the structural transition to lower temperature.

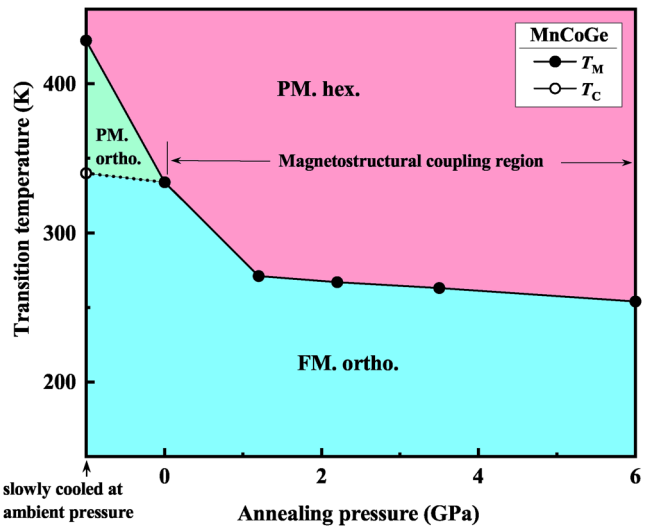

FIG. 6. Magnetic and structural phase diagram of MnCoGe as a function of annealing pressure and temperature, where all samples were annealed at 800 °C followed by rapid cooling. The abbreviations "ortho." and "hex." refer to the orthorhombic and hexagonal crystal structures, respectively.

paramagnetic state, which is not detectable in the magnetization measurement. Note that the heat flow data measured during heating and cooling processes with a ramp rate of 2 K/min have been corrected for baseline drift. According to the DSC results, the sample SC_0 undergoes forward and reverse structural transitions at T = 415 and 443 K, respectively, with a thermal hysteresis of $\Delta T_{hyst} = 28$ K. This is consistent with previously reported results.[8]

For MnCoGe rapidly cooled at ambient pressure (RC_0), the structural transition significantly shifted to a lower temperature ($T_M = 334$ K) and merged with the magnetic transition to form a first-order magnetostructural transition (MST). The first-order nature of this transition is clearly demonstrated by the considerable thermal hysteresis between the heating and cooling curves (see Fig. 5). When the rapid cooling occurred under pressures of 1.2 (RC_1.2), 2.2 (RC_2.2), 3.5 (RC_3.5), and 6.0 GPa (RC_6.0), the structural transition continuously shifted to lower temperatures while still coinciding with the magnetic transition, i.e., they were still coupled.

The significant shift in structural transition in rapidly cooled samples at ambient pressure as well as under high pressure relative to that of a slow-cooled sample could be associated with the disordered structure caused by quenching and applied pressure. As reported in the literature, the structural transition in MnCoGe is sensitive to annealing temperature, cooling procedures followed by annealing, and applied physical pressure.[48,67] Moreover, Caron *et al.*[42] reported that the magnetocrystalline coupling present in the MnCoGe-based compound is more easily driven by crystallographic change. When MnCoGe is allowed to cool slowly (at a rate of 0.5 C/min) after annealing at 800 °C, the transformation from the high-temperature hexagonal to low-temperature orthorhombic phases completes naturally above room temperature. However, rapid cooling, i.e., quenching, induces a remnant strain resulting in lattice distortion. This may lead to a strengthening of the covalent bonds between Mn–Mn atoms by reducing the Mn–Mn interlayer distance, which is considered a major factor in driving the structural transition to a lower temperature in MnCoGe-based compounds.[68]

Similar to the thermal treatment procedure, physically applied pressure also stabilizes the high-temperature hexagonal phase in MnCoGe by lowering its structural transition temperature. This is seen directly when pressure is applied during measurement (rather than during synthesis).[48] This change in transition temperature is also attributed to the reduction in Mn–Mn interlayer distance and strengthening of the covalent bond due to applied pressure.[65] When both quenching and physical pressure act simultaneously on a sample, cumulative effects are likely to occur, leading to a greater degree of internal strain and lattice distortion in the sample

26 December 2024 02:38:23

© Author(s) 2024

compared to that induced by quenching alone. Consequently, a larger reduction in Mn–Mn interlayer distance can be expected, which in turn further decreases the magnetostructural transition temperature in samples rapidly cooled under high pressures relative to those quenched at ambient pressure. The continuous shift in magnetostructural transition with increasing annealing pressure in high-pressure annealed samples are likely due to the increased pressure-induced lattice distortion. The structural transition temperatures obtained from the magnetization measurements are in agreement with the XRD results shown in Fig. 2.

In Fig. 5, it can also be noticed that the magnetostructural transition in high-pressure annealed samples became broadened and less sharp in comparison to those of the heat-treated samples at ambient pressure. It is reported in the literature that the structural transition in MnCoGe-based compounds is usually broadened due to the application of physical pressure, and its cause is mainly attributed to the pressure-induced residual strain, which affects the martensitic transformation.[69] A similar cause might be responsible for the broadening of the magentostructural transition in high-pressure annealed samples in this study. Furthermore, an earlier investigation shows that an increase in applied hydrostatic pressure continuously drives the magnetostructural transition to a lower temperature in MnCoGe, and the decoupling of its magnetic and structural transition occurs when the pressure is sufficiently high ($\geq$7.9 kbar).[48] In the current study, the high-pressure annealed samples might be on the verge of decoupling (or have partially decoupled) their magnetic and structural transitions, resulting in a notable broadening and two-step like feature of the magnetostructural transition. In any case, the significance of these magnetization results is that magentostructural transitions can be established in stoichiometric MnCoGe without altering its composition by varying the thermal processing pressure. This can lead to significant magnetocaloric effects near room temperature, despite the conventionally synthesized material showing negligible such effects.

Figure 6 shows the annealing pressure dependence of the structural and magnetic phase diagrams, which were constructed using the XRD, DSC, and magnetization data. Here, the structural transition temperature (T_M) represents an average of the forward and reverse structural transition temperatures, which were evaluated from the peaks of the derivatives of the M–T curves. Note that

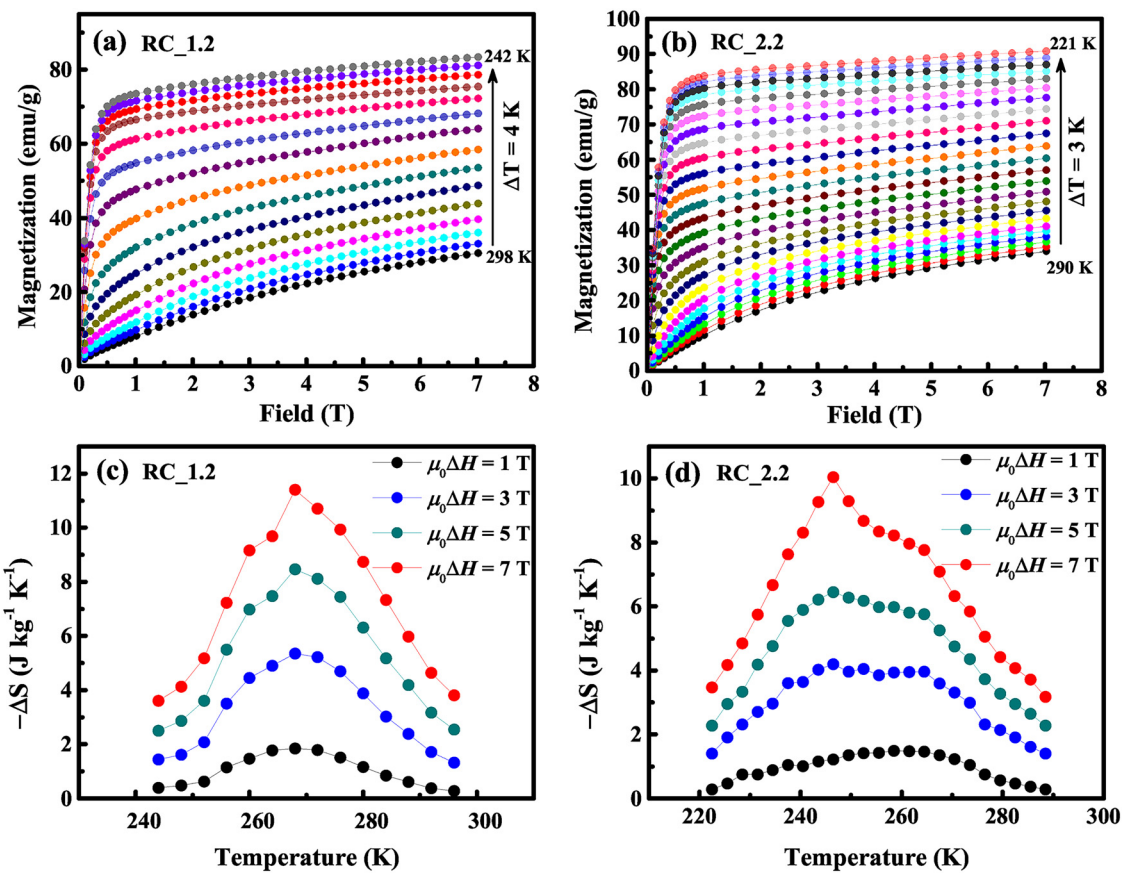

FIG. 7. Isothermal magnetization measurements performed at different temperatures near the magnetostructural transitions for samples (a) RC_1.2 and (b) RC_2.2. Temperature dependence of magnetic entropy change for the samples (c) RC_1.2 and (d) RC_2.2 for field changes of $\mu_0\Delta H$ = 1, 3, 5, and 7 T.

26 December 2024 02:38:23

© Author(s) 2024

T_M was determined from the heat flow data for the sample SC_0. The structural transition temperatures for all samples are provided in Table I. Similarly, the magnetic transition temperature is defined as the point where the slope of the M–T curve reaches its maximum. In Fig. 6, it can be seen that the structural transition temperature decreases with increasing thermal processing pressure. Furthermore, a noteworthy observation is the coexistence of the magnetic and structural transitions, resulting in a first-order magnetostructural transition (MST) between the FM orthorhombic and PM hexagonal phases in a wide range of temperatures from 254 to 334 K. This behavior causes the magnetocaloric effects to occur on the periphery of room temperature, which is advantageous for practical applications.

The strong spin-lattice coupling often results in large magnetocaloric effects in these materials, where the contribution of the latent heat of the first-order transition is significant.[70,71] Here, the MCEs were characterized in samples RC_1.2 and RC_2.2 by evaluating their isothermal magnetic entropy changes (ΔS_M), which is one of the parameters that quantifies magnetocaloric properties of a material. For this, we performed a set of isothermal magnetization measurements [$M(H)$] at different temperatures in fields up to 7 T, with the temperature being incrementally changed across the magnetostructural transition, as shown in Figs. 7(a) and 7(b). The $M(H)$ curves were measured using the "loop process method," where the sample was gradually cooled from the high-temperature PM phase to the desired measurement temperature in the zero magnetic field before each isothermal magnetization measurement.[72,73] This procedure effectively prevents the occurrence of the so-called "peak effect" and allows for precise determination of ΔS_M during the magnetostructural transition, even when there is a thermal hysteresis. The magnetic entropy changes were then calculated employing the thermodynamic relation,

$$\Delta S_M(T, \Delta H) = \int_0^H \left(\frac{\partial M(T, H')}{\partial T}\right)_H dH' \cong \frac{1}{\Delta T}\left[\int_0^H M(T+\Delta T, H')\, dH' - \int_0^H M(T, H')\, dH'\right].$$

Figures 7(c) and 7(d) show the temperature-dependent isothermal magnetic entropy changes ($-\Delta S_M$) for field changes of $\mu_0\Delta H = 1$, 3, 5, and 7 T for samples RC_1.2 and RC_2.2. The magnetic entropy changes in both samples are of comparable magnitude, but their peaks occurred at different temperatures. For the sample RC_1.2, the maximum ΔS_M for a field change of $\mu_0\Delta H = 7$ T is $-11.4\ \mathrm{J\,kg^{-1}\,K^{-1}}$, and its full width at half maximum of the entropy is $\delta_{FWHM} \cong 30$ K. Similarly, the maximum ΔS_M of $-10.0\ \mathrm{J\,kg^{-1}\,K^{-1}}$ for 7 T field change was observed in the sample RC_2.2, and its corresponding δ_{FWHM} is 42 K. These significant values of ΔS_M are a consequence of magnetostructural transitions induced by high-pressure annealing in both samples. Furthermore, the relative cooling power (RCP), another parameter used to assess the magnetocaloric effectiveness of material, was estimated for both samples using the relation, $\mathrm{RCP} = |\Delta S|_{max} \times \delta_{FWHM}$. For RC_1.2, the RCP is $\approx 342\ \mathrm{J\,kg^{-1}}$ for $\mu_0\Delta H = 7$ T, while its value increased to $\approx 420\ \mathrm{J\,kg^{-1}}$ in the sample RC_2.2. These results show that high-pressure annealing can act as an effective method to induce large magnetocaloric effects in MnCoGe.

IV. CONCLUSIONS

In conclusion, the effects of high-pressure annealing on the structural, magnetic, and magnetocaloric properties of stoichiometric MnCoGe were investigated. It was found that, as the annealing pressure increased, the structural transition shifted to lower temperature, locking the hexagonal structure in a metastable phase. A considerable deformation in the crystal structure was observed across the structural transition, resulting in a significant change in unit cell volume (~4.2%). A magnetostructural transition between the FM orthorhombic and PM hexagonal phases was established in stoichiometric MnCoGe, which can be tuned over a wide range of temperatures (>80 K) by adjusting the annealing pressure, and resulted in considerable magnetic entropy changes (up to $11.4\ \mathrm{J\,kg^{-1}\,K^{-1}}$ for $\mu_0\Delta H = 7$ T) and large relative cooling powers (up to ≈ 420 J/kg) near room temperature. These results established the approach of applying high pressure during thermal processing/synthesis as an effective method to tailor the magnetocaloric properties of materials without changing their compositions. Moreover, our findings may pave the way for the development of new functional materials in the field of magnetocaloric cooling.

ACKNOWLEDGMENTS

S. Stadler acknowledges support from the U.S. Department of Energy (DOE), Office of Basic Energy Sciences under Award No. DE-FG02-13ER46946. N. Ali, I. Dubenko, and S. Talapatra acknowledge support from the U.S. Department of Energy (DOE), Office of Basic Energy Sciences under Award No. DE-FG02-06ER46291. D. P. Young acknowledges support from the U.S. National Science Foundation (NSF), Division of Materials Research under Award No. NSF-DMR-1904636. The DSC measurement presented in this work was carried out at the Center for Advanced Microstructures and Devices (CAMD) under the supervision of A. Roy.

26 December 2024 02:38:23

AUTHOR DECLARATIONS

Conflict of Interest

The authors have no conflicts to disclose.

Author Contributions

Tej Poudel Chhetri: Conceptualization (equal); Formal analysis (equal); Investigation (equal); Methodology (equal); Writing – original draft (equal). **Jing-Han Chen:** Investigation (equal); Methodology (equal); Writing – review & editing (equal). **David P. Young:** Funding acquisition (equal); Methodology (equal); Resources (equal); Writing – review & editing (equal). **Igor Dubenko:** Writing – review & editing (equal). **Saikat Talapatra:** Funding acquisition (equal); Resources (equal); Writing – review & editing (equal). **Naushad Ali:** Funding acquisition (equal); Resources (equal); Writing – review & editing (equal). **Shane Stadler:** Conceptualization (equal); Funding acquisition (equal); Investigation (equal); Project administration (equal); Resources (equal); Supervision (equal); Writing – review & editing (equal).

© Author(s) 2024

DATA AVAILABILITY

The data that support the findings of this study are available from the corresponding author upon reasonable request.

REFERENCES

[1]C. Zhang, H. Shi, E. Ye, Y. Nie, Z. Han, B. Qian, and D. Wang, Appl. Phys. Lett. **107**, 212403 (2015).
[2]N. Trung, L. Zhang, L. Caron, K. Buschow, and E. Brück, Appl. Phys. Lett. **96**, 172504 (2010).
[3]A. Biswas, A. K. Pathak, N. A. Zarkevich, X. Liu, Y. Mudryk, V. Balema, D. D. Johnson, and V. K. Pecharsky, Acta Mater. **180**, 341 (2019).
[4]T. Samanta, I. Dubenko, A. Quetz, S. Stadler, and N. Ali, Appl. Phys. Lett. **101**, 242405 (2012).
[5]L. Li and M. Yan, J. Alloys Compd. **823**, 153810 (2020).
[6]K. Koyama, M. Sakai, T. Kanomata, and K. Watanabe, Jpn. J. Appl. Phys. **43**, 8036 (2004).
[7]P. Dutta, S. Pramanick, V. Singh, D. T. Major, D. Das, and S. Chatterjee, Phys. Rev. B **93**, 134408 (2016).
[8]Y.-Y. Zhao, F.-X. Hu, L.-F. Bao, J. Wang, H. Wu, Q.-Z. Huang, R.-R. Wu, Y. Liu, F.-R. Shen, H. Kuang *et al.*, J. Am. Chem. Soc. **137**, 1746 (2015).
[9]Q. Ren, W. Hutchison, J. Wang, A. Studer, G. Wang, H. Zhou, J. Ma, and S. J. Campbell, ACS Appl. Mater. Interfaces **11**, 17531 (2019).
[10]W. Guo, X. Miao, Z. Yan, Y. Chen, Y. Gong, F. Qian, F. Xu, and L. Caron, Mater. Res. Lett. **12**, 315 (2024).
[11]P. Von Ranke, N. De Oliveira, C. Mello, A. M. G. Carvalho, and S. Gama, Phys. Rev. B **71**, 054410 (2005).
[12]V. Johnson, Inorg. Chem. **14**, 1117 (1975).
[13]W. Bazela, A. Szytuła, J. Todorović, Z. Tomkowicz, and A. Zięba, Phys. Status Solidi A **38**, 721 (1976).
[14]A. Szytuła, W. Bażla, and S. Radenković, J. Magn. Magn. Mater. **38**, 99 (1983).
[15]E. Liu, W. Wang, L. Feng, W. Zhu, G. Li, J. Chen, H. Zhang, G. Wu, C. Jiang, H. Xu *et al.*, Nat. Commun. **3**, 873 (2012).
[16]J. Liu, Y. Gong, G. Xu, G. Peng, I. A. Shah, N. Ul Hassan, and F. Xu, Sci. Rep. **6**, 23386 (2016).
[17]A. Quetz, T. Samanta, I. Dubenko, M. J. Kangas, J. Y. Chan, S. Stadler, and N. Ali, J. Appl. Phys. **114**, 153909 (2013).
[18]S. K. Pal, C. Frommen, S. Kumar, B. Hauback, H. Fjellvåg, T. Woodcock, K. Nielsch, and G. Helgesen, J. Alloys Compd. **775**, 22 (2019).
[19]T. Poudel Chhetri, J.-H. Chen, A. T. Grant, D. P. Young, I. Dubenko, S. Talapatra, N. Ali, and S. Stadler, J. Appl. Phys. **132**, 045107 (2022).
[20]S. Ma, Y. Zheng, H. Xuan, L. Shen, Q. Cao, D. Wang, Z. Zhong, and Y. Du, J. Magn. Magn. Mater. **324**, 135 (2012).
[21]X. Si, Y. Shen, X. Ma, S. Chen, J. Lin, J. Yang, T. Gao, and Y. Liu, Acta Mater. **143**, 306 (2018).
[22]J. Hamer, R. Daou, S. Özcan, N. Mathur, D. Fray, and K. Sandeman, J. Magn. Magn. Mater. **321**, 3535 (2009).
[23]G. Li, E. Liu, H. Zhang, Y. Zhang, J. Chen, W. Wang, H. Zhang, G. Wu, and S. Yu, J. Magn. Magn. Mater. **332**, 146 (2013).
[24]E. Liu, H. Zhang, G. Xu, X. Zhang, R. Ma, W. Wang, J. Chen, H. Zhang, G. Wu, L. Feng *et al.*, Appl. Phys. Lett. **102**, 122405 (2013).
[25]D. Zhang, Z. Nie, Z. Wang, L. Huang, Q. Zhang, and Y.-D. Wang, J. Magn. Magn. Mater. **387**, 107 (2015).
[26]A. Aryal, A. Quetz, S. Pandey, T. Samanta, I. Dubenko, M. Hill, D. Mazumdar, S. Stadler, and N. Ali, J. Alloys Compd. **709**, 142 (2017).
[27]J.-H. Chen, A. Trigg, T. Poudel Chhetri, D. P. Young, I. Dubenko, N. Ali, and S. Stadler, J. Appl. Phys. **127**, 213901 (2020).
[28]J. Liu, Y. Gong, Y. You, X. You, B. Huang, X. Miao, G. Xu, F. Xu, and E. Brück, Acta Mater. **174**, 450 (2019).
[29]Y. Kuang, B. Yang, X. Hao, H. Xu, Z. Li, H. Yan, Y. Zhang, C. Esling, X. Zhao, and L. Zuo, J. Magn. Magn. Mater. **506**, 166782 (2020).
[30]C. Zhang, D. Wang, Z. Han, B. Qian, H. Shi, C. Zhu, J. Chen, and T. Wang, Appl. Phys. Lett. **103**, 132411 (2013).
[31]K. Deepak and R. Ramanujan, J. Alloys Compd. **743**, 494 (2018).
[32]Z.-Y. Wei, E.-K. Liu, Y. Li, G.-Z. Xu, X.-M. Zhang, G.-D. Liu, X.-K. Xi, H.-W. Zhang, W.-H. Wang, G.-H. Wu *et al.*, Adv. Electron. Mater. **1**, 1500076 (2015).
[33]J. Liu, K. Skokov, and O. Gutfleisch, Scr. Mater. **66**, 642 (2012).
[34]C. Zhang, D. Wang, Q. Cao, Z. Han, H. Xuan, and Y. Du, Appl. Phys. Lett. **93**, 122505 (2008).
[35]Y. Fang, C. Yeh, C. Chang, W. Chang, M. Zhu, and W. Li, Scr. Mater. **57**, 453 (2007).
[36]E. Liu, W. Zhu, L. Feng, J. Chen, W. Wang, G. Wu, H. Liu, F. Meng, H. Luo, and Y. Li, Europhys. Lett. **91**, 17003 (2010).
[37]T. Samanta, P. Lloveras, A. Us Saleheen, D. L. Lepkowski, E. Kramer, I. Dubenko, P. W. Adams, D. P. Young, M. Barrio, J. L. Tamarit *et al.*, Appl. Phys. Lett. **112**, 021907 (2018).
[38]S. Ghosh, A. Ghosh, P. Sen, and K. Mandal, Phys. Rev. Appl. **14**, 014016 (2020).
[39]S. Anzai and K. Ozawa, Phys. Rev. B **18**, 2173 (1978).
[40]V. Sharma, N. Garg, and M. Manekar, AIP Adv. **12**, 035107 (2022).
[41]T. Samanta, D. L. Lepkowski, A. U. Saleheen, A. Shankar, J. Prestigiacomo, I. Dubenko, A. Quetz, I. W. Oswald, G. T. McCandless, J. Y. Chan *et al.*, J. Appl. Phys. **117**, 123911 (2015).
[42]L. Caron, N. Trung, and E. Brück, Phys. Rev. B **84**, 020414 (2011).
[43]Q. Y. Ren, W. D. Hutchison, J. L. Wang, A. J. Studer, and S. J. Campbell, J. Alloys Compd. **693**, 32 (2017).
[44]Y. Li, Q. Zeng, Z. Wei, E. Liu, X. Han, Z. Du, L. Li, X. Xi, W. Wang, S. Wang *et al.*, Acta Mater. **174**, 289 (2019).
[45]J.-H. Chen, T. P. Chhetri, A. U. Saleheen, D. P. Young, I. Dubenko, N. Ali, and S. Stadler, Intermetallics **112**, 106547 (2019).
[46]C. Zhang, Y. Nie, H. Shi, E. Ye, Z. Han, and D. Wang, J. Magn. Magn. Mater. **469**, 437 (2019).
[47]K. Noguchi, R. Kobayashi, Y. Mitsui, R. Y. Umetsu, J. Gouchi, Y. Uwatoko, and K. Koyama, J. Magn. Magn. Mater. **499**, 166199 (2020).
[48]J.-H. Chen, T. Poudel Chhetri, C.-K. Chang, Y.-C. Huang, D. P. Young, I. Dubenko, S. Talapatra, N. Ali, and S. Stadler, J. Appl. Phys. **129**, 215108 (2021).
[49]J.-H. Chen, T. Poudel Chhetri, A. T. Grant, X. Bai, Q. Zhang, C.-K. Chang, D. P. Young, I. Dubenko, S. Talapatra, N. Ali *et al.*, J. Phys. D: Appl. Phys. **57**, 205003 (2024).
[50]R. Wu, F. Shen, F. Hu, J. Wang, L. Bao, L. Zhang, Y. Liu, Y. Zhao, F. Liang, W. Zuo *et al.*, Sci. Rep. **6**, 20993 (2016).
[51]C. F. Sánchez-Valdés, J. S. Llamazares, H. Flores-Zúñiga, D. Ríos-Jara, P. Alvarez-Alonso, and P. Gorria, Scr. Mater. **69**, 211 (2013).
[52]Y. Xiao, F. Qian, X. Gao, R. Zhao, X. Miao, and H. Yang, Ceram. Int. **49**, 18180 (2023).
[53]L. Zhang, S. Ma, Q. Ge, K. Liu, Q. Jiang, X. Han, S. Yang, K. Yu, and Z. Zhong, J. Mater. Sci. Technol. **33**, 1362 (2017).
[54]W. Matizamhuka, *Sintering of Functional Materials*, edited by Igor V. Shishkovsky, p. 165–182 (2018).
[55]J. Liu, Y. Si, Y. Gong, G. Xu, E. Liu, F. Xu, and D. Wang, J. Alloys Compd. **701**, 858 (2017).
[56]C. Wang, Q. Hu, L. Zhang, and M. Wei, Philos. Mag. **101**, 964 (2021).
[57]T. Poudel Chhetri, J.-H. Chen, A. T. Grant, D. P. Young, I. Dubenko, S. Talapatra, N. Ali, and S. Stadler, J. Appl. Phys. **133**, 065104 (2023).
[58]S. Ma, H. Xuan, C. Zhang, L. Wang, Q. Cao, D. Wang, and Y. Du, Appl. Phys. Lett. **97**, 052506 (2010).
[59]S. Ma, D. Wang, Z. Zhong, J. Luo, J. Xu, and Y. Du, Appl. Phys. Lett. **102**, 032407 (2013).
[60]S. Lin, O. Tegus, E. Bruck, W. Dagula, T. Gortenmulder, and K. Buschow, IEEE Trans. Magn. **42**, 3776 (2006).
[61]K. Momma and F. Izumi, J. Appl. Crystallogr. **44**, 1272 (2011).
[62]H. M. Rietveld, J. Appl. Crystallogr. **2**, 65 (1969).
[63]B. H. Toby, J. Appl. Crystallogr. **34**, 210 (2001).

26 December 2024 02:38:23

© Author(s) 2024

[64]S. Nizioł, A. Wesełucha, W. Bażela, and A. Szytuła, Solid State Commun. **39**, 1081 (1981).
[65]R.-R. Wu, L.-F. Bao, F.-X. Hu, H. Wu, Q.-Z. Huang, J. Wang, X.-L. Dong, G.-N. Li, J.-R. Sun, F.-R. Shen *et al.*, Sci. Rep. **5**, 18027 (2015).
[66]Q. Ren, W. D. Hutchison, J. Wang, A. J. Studer, and S. J. Campbell, Chem. Mater. **30**, 1324 (2018).
[67]J. Torrens-Serra, C. Biffi, R. Santamarta, V. Recarte, J. Pérez-Landazábal, A. Tuissi, and E. Cesari, Mater. Charact. **93**, 24 (2014).
[68]X. Miao, Y. Gong, L. Caron, Y. You, G. Xu, D. Sheptyakov, P. Manuel, F. Qian, Y. Zhang, F. Xu *et al.*, Phys. Rev. Mater. **4**, 104407 (2020).
[69]Y. Liu, F. Shen, M. Zhang, L. Bao, R. Wu, Y. Zhao, F. Hu, J. Wang, W. Zuo, J. Sun *et al.*, J. Alloys Compd. **649**, 1048 (2015).
[70]J. Liu, T. Gottschall, K. P. Skokov, J. D. Moore, and O. Gutfleisch, Nat. Mater. **11**, 620 (2012).
[71]F. Guillou, G. Porcari, H. Yibole, N. van Dijk, and E. Brück, Adv. Mater. **26**, 2671 (2014).
[72]L. Caron, Z. Ou, T. Nguyen, D. C. Thanh, O. Tegus, and E. Brück, J. Mag. Magn. Mater. **321**, 3559 (2009).
[73]J.-H. Chen, A. Us Saleheen, P. W. Adams, D. P. Young, N. Ali, and S. Stadler, J. Appl. Phys. **123**, 145101 (2018).

26 December 2024 02:38:23

© Author(s) 2024